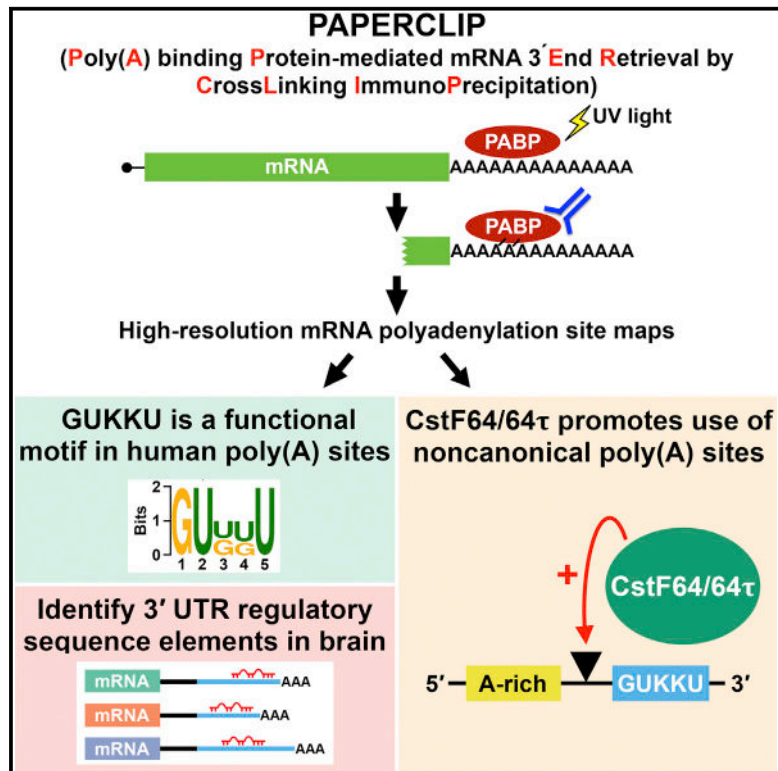


Cell Reports

PAPERCLIP Identifies MicroRNA Targets and a Role of CstF64/64tau in Promoting Non-canonical poly(A) Site Usage

Graphical Abstract



Authors

Hun-Way Hwang, Christopher Y. Park, Hani Goodarzi, ..., Michael J. Moore, Yuhki Saito, Robert B. Darnell

Correspondence

hhwang@rockefeller.edu (H.-W.H.), darnelr@rockefeller.edu (R.B.D.)

In Brief

Hwang et al. develop PAPERCLIP, a high-performance mRNA 3' end mapping method based on the CLIP technique. They use PAPERCLIP to show that CstF64/64tau promotes non-canonical poly(A) site usage through a GUKKU motif. Furthermore, they also discover shifts in alternative polyadenylation and identify novel microRNA binding sites during mouse brain development.

Highlights

- PAPERCLIP is a high-performance mRNA 3' end mapping method based on the CLIP technique
- PAPERCLIP provides insights into the regulation of alternative polyadenylation
- PAPERCLIP expands knowledge of 3'-UTR-mediated mRNA regulation

Accession Numbers

GSE66092



Hwang et al., 2016, Cell Reports 15, 423–435
April 12, 2016 ©2016 The Authors
<http://dx.doi.org/10.1016/j.celrep.2016.03.023>

CellPress

PAPERCLIP Identifies MicroRNA Targets and a Role of CstF64/64tau in Promoting Non-canonical poly(A) Site Usage

Hun-Way Hwang,^{1,*} Christopher Y. Park,^{1,2} Hani Goodarzi,³ John J. Fak,¹ Aldo Mele,^{1,4} Michael J. Moore,¹ Yuhki Saito,¹ and Robert B. Darnell^{1,2,*}

¹Laboratory of Molecular Neuro-Oncology and Howard Hughes Medical Institute, The Rockefeller University, 1230 York Avenue, New York, New York 10065, USA

²New York Genome Center, 101 Avenue of the Americas, New York, NY 10013, USA

³Laboratory of Systems Cancer Biology, The Rockefeller University, 1230 York Avenue, New York, New York 10065, USA

⁴Present address: Horizon Discovery, 7100 Cambridge Research Park, Waterbeach, Cambridge CB25 9TL, UK

*Correspondence: hhwang@rockefeller.edu (H.-W.H.), darnellr@rockefeller.edu (R.B.D.)

<http://dx.doi.org/10.1016/j.celrep.2016.03.023>

SUMMARY

Accurate and precise annotation of 3' UTRs is critical for understanding how mRNAs are regulated by microRNAs (miRNAs) and RNA-binding proteins (RBPs). Here, we describe a method, poly(A) binding protein-mediated mRNA 3' end retrieval by crosslinking immunoprecipitation (PAPERCLIP), that shows high specificity for mRNA 3' ends and compares favorably with existing 3' end mapping methods. PAPERCLIP uncovers a previously unrecognized role of CstF64/64tau in promoting the usage of a selected group of non-canonical poly(A) sites, the majority of which contain a downstream GUKKU motif. Furthermore, in the mouse brain, PAPERCLIP discovers extended 3' UTR sequences harboring functional miRNA binding sites and reveals developmentally regulated APA shifts, including one in *Atp2b2* that is evolutionarily conserved in humans and results in the gain of a functional binding site of miR-137. PAPERCLIP provides a powerful tool to decipher post-transcriptional regulation of mRNAs through APA in vivo.

INTRODUCTION

The 3' UTRs of mRNAs often contain sequence elements to interact with regulators such as microRNAs (miRNAs) and RNA-binding proteins (RBPs) (Elkon et al., 2013; Licatalosi and Darnell, 2010). Through alternative polyadenylation (APA), cells and tissues are able to fine-tune gene expression by altering the inclusion of 3' UTR regulatory elements to allow or deny access to regulators (Di Giammartino et al., 2011). Therefore, accurate and precise annotation of the 3' UTRs is critical for understanding how mRNA stability, localization, and translational efficiency are regulated by miRNAs and RBPs.

mRNA 3' end mapping is commonly performed by reverse-transcribing mRNAs from the poly(A) tails, utilizing oligo(dT)

primers to construct the sequencing library (hereafter referred to as "3' end sequencing"). Different varieties of this approach, such as PAS-seq, PolyA-seq, 3' Seq, and 3'-seq (different from the former) have been described recently in the literature (Derti et al., 2012; Jenal et al., 2012; Lianoglou et al., 2013; Shepard et al., 2011). (For a more complete list, see a recent review by Shi, 2012.) However, the oligo(dT) primers also anneal to internal adenine-rich sequences in mRNA, which results in mispriming during reverse transcription (Di Giammartino et al., 2011; Nam et al., 2002). The presence of internal priming events, which may represent 30% of the entire library (Derti et al., 2012), diminishes the effective sequencing depth and requires strict in silico filtering to improve accuracy.

Different filtering strategies have been developed to remove potential internal priming events (Derti et al., 2012; Shepard et al., 2011). One commonly used filtering strategy is to remove reads mapping immediately upstream of genomic adenine-rich regions because they likely arise from mispriming events. However, these manipulations remove many authentic poly(A) sites in addition to misprimed sites (Hoque et al., 2013), and different algorithms exhibit distinct biases (Derti et al., 2012). To minimize false positives, studies utilizing 3' end sequencing are inclined to be conservative about poly(A) site annotations, which diminishes the possibility of identifying novel poly(A) sites and limits the scope of study.

To improve mRNA 3' end mapping, we applied the crosslinking immunoprecipitation (CLIP) technique to poly(A)-binding protein, a factor with high specificity for mRNA poly(A) tails (Kahvejian et al., 2001). CLIP captures direct RNA-protein interaction in situ, allowing stringent immunopurification that effectively eliminates non-specific interactions to generate precise genome-wide interaction maps (Licatalosi et al., 2008). Our method, poly(A) binding protein-mediated mRNA 3' end retrieval by crosslinking immunoprecipitation (PAPERCLIP), minimizes the internal priming problem without utilizing in silico filtering and allows unbiased discovery of mRNA 3' ends. We performed extensive validation to show that PAPERCLIP has high specificity for mRNA 3' ends and generates comprehensive maps of poly(A) sites at nucleotide resolution. Functional analysis using PAPERCLIP discovered a previously unrecognized role

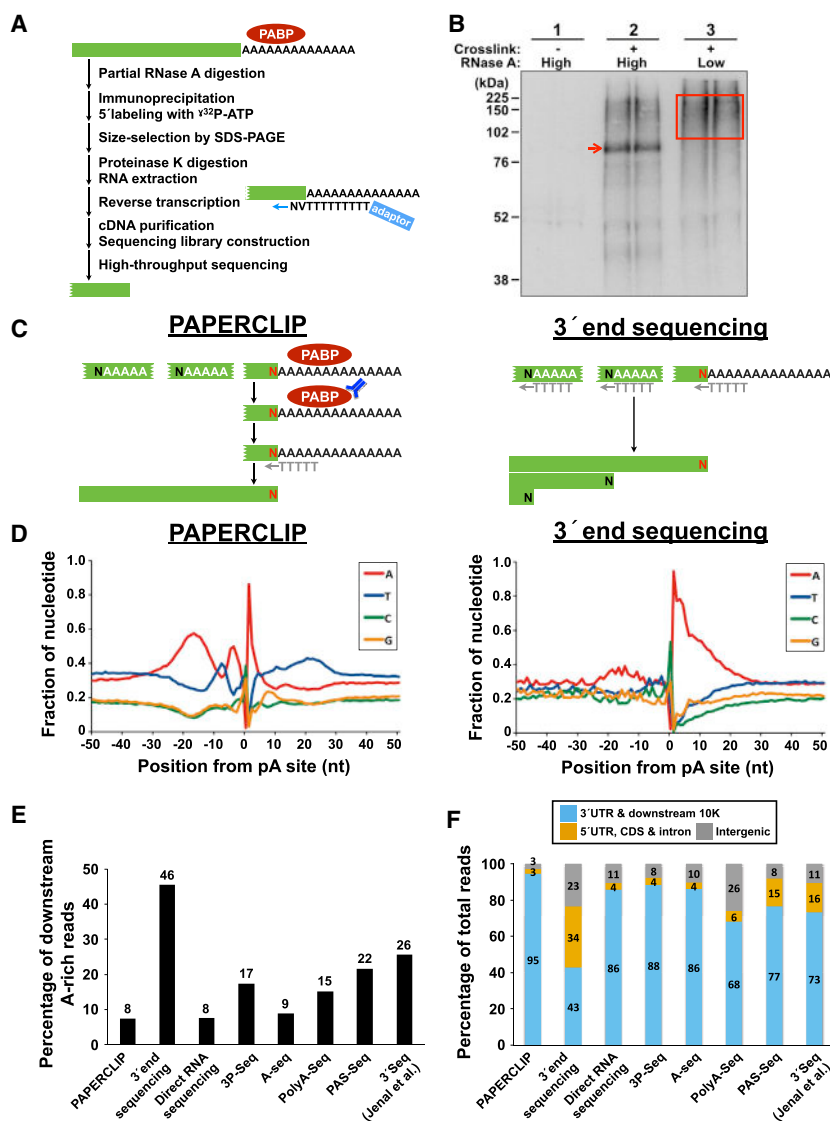


Figure 1. PAPERCLIP Ameliorates the Internal Priming Problem Commonly Seen in 3' End Sequencing and Compares Favorably with Other 3' End Mapping Methods

(A) Diagram for the PAPERCLIP protocol.

(B) Autoradiogram from the PAPERCLIP experiment. The red arrow denotes the PABP-RNA complex. The red box shows the area of the nitrocellulose membrane used for RNA extraction and subsequent sequencing library construction.

(C) Schematics illustrating the difference between PAPERCLIP (left) and 3' end sequencing (right).

(D) Diagrams showing the genomic nucleotide sequence surrounding the putative poly(A) sites identified by PAPERCLIP (left) and 3' end sequencing (right) in HeLa cells.

(E) Bar graph showing the percentage of downstream adenine-rich reads for different 3' end mapping methods. The data for PAPERCLIP and 3' end sequencing are from this study, whereas the data for the other methods were obtained from the NCBI.

(F) Bar graph showing the percentage of reads mapped to different genomic regions. The data sources are the same as in (E). CDS, coding DNA sequence.

the internal adenine-rich fragments are excluded from the final sequencing library (Figure 1C). As a result, stringent sequence-based or genomic location-based filtering is not necessary, allowing the poly(A) sites to be mapped in an unbiased manner.

To directly compare PAPERCLIP to 3' end sequencing, we used a 3' end sequencing protocol adapted from the 3' Seq protocol (Jenal et al., 2012) and performed both methods to map poly(A) sites in HeLa cells (library statistics are provided in Table S1). Consistent with previous reports (Derti et al., 2012; Wang et al., 2013), the 3' end sequencing library contained a large number of internal priming events prior to filtering, as

of CstF64/64tau in promoting the usage of non-canonical poly(A) sites. We further combined PAPERCLIP and Argonaute (Ago) high-throughput sequencing of RNA isolated by crosslinking immunoprecipitation (HITS-CLIP) (Chi et al., 2009) in both adult and developing mouse brain to discover regulatory relationships between mRNAs and miRNAs, demonstrating the capacity of PAPERCLIP to provide critical knowledge for understanding post-transcriptional regulation of mRNAs in vivo.

RESULTS

PAPERCLIP Ameliorates the Internal Priming Problem

To develop an alternative strategy to globally map mRNA 3' ends with high specificity, we took advantage of the well documented property of PABP, which is its high selectivity for the poly(A) tails of mRNAs (Kahvejian et al., 2001), to develop PAPERCLIP (Figures 1A and 1B). In PAPERCLIP, only mRNA fragments containing the poly(A) tail are retained by crosslinking to PABP, whereas

evidenced by the strong enrichment of adenines immediately downstream of putative poly(A) sites in the human genome (Figure 1D, right). In contrast, the composition of nucleotide sequence surrounding poly(A) sites identified by PAPERCLIP is devoid of downstream genomic adenines and is highly similar to the nucleotide composition at mRNA 3' ends mapped by direct RNA sequencing (Ozsolak et al., 2010; Figure 1D, left). These results demonstrate that PAPERCLIP is highly specific for the mRNA 3' ends and ameliorates the internal priming problem seen in the 3' end sequencing.

We next compared PAPERCLIP to other 3' end mapping methods using publicly available data (library statistics are provided in Table S1). To evaluate the performance without in silico filtering, all uniquely mapped reads from each method were used for comparison. We first counted the number of reads that were aligned immediately upstream to genomic adenine-rich regions, a method commonly used to estimate the occurrence of internal priming events (Derti et al., 2012; Shepard

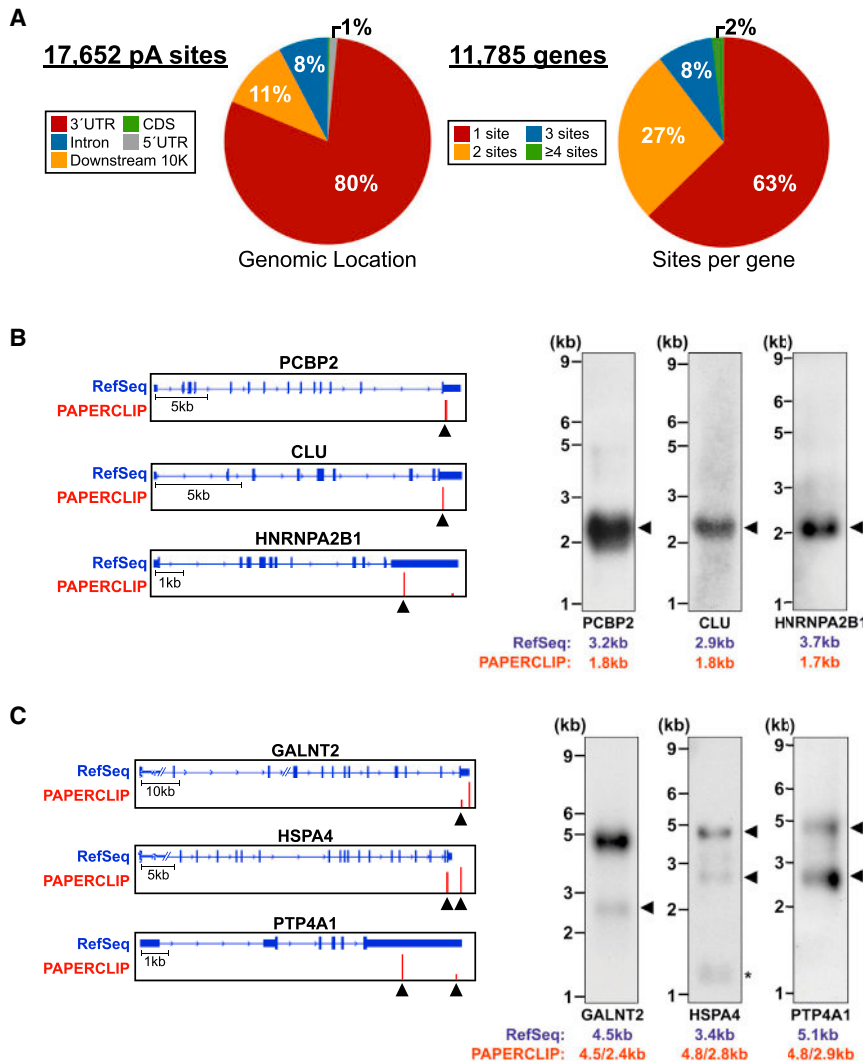


Figure 2. PAPERCLIP Depicts a High-Resolution, Comprehensive mRNA Polyadenylation Map of HeLa Cells

(A) Pie charts showing the genomic location (left) and the per gene distribution (right) of poly(A) sites identified by PAPERCLIP in HeLa cells. (B and C) Left: diagrams showing RefSeq annotation and PAPERCLIP results. The peak heights from PAPERCLIP are scaled for each gene. Right: results from validating northern blot experiments. The numbers below denote the expected sizes of transcripts from RefSeq annotation and PAPERCLIP results. The arrowheads indicate poly(A) sites not present in the RefSeq annotation for the diagram and the corresponding mRNA isoforms for the northern blots.

between the two replicates (Figure S1B) and the fact that the vast majority (15,176, 86%) of 17,652 poly(A) sites were annotated at the identical nucleotide position in both replicates (Figure S1C). Consistent with previous reports (Derti et al., 2012; Nam et al., 2014), we observed a considerable difference between the RefSeq annotation (June 2014) and the poly(A) sites identified by PAPERCLIP. Of all 11,785 annotated genes detected in HeLa cells, 6,666 genes (57%) had at least one poly(A) site that was not present in the RefSeq annotation and 3,756 (32%) genes exclusively use non-RefSeq poly(A) sites. To validate the results from PAPERCLIP, we first performed northern blotting and detected mRNAs at the expected size based on PAPERCLIP annotation (Figures 2B and 2C). Although it is known that RNA sequencing (RNA-seq) lacks sufficient

et al., 2011). Of all methods that were compared, PAPERCLIP and direct RNA sequencing had the lowest percentage of downstream adenine-rich reads (Figure 1E). We next compared the genomic localization of the mapped reads. Overall, PAPERCLIP had the strongest enrichment of reads in annotated 3' UTRs and 10 kb downstream of annotated genes in addition to the lowest percentage of intergenic reads (Figure 1F). Taken together, these results provide strong evidence that PAPERCLIP not only minimizes the internal priming problem but also compares favorably with many other 3' end mapping methods, including direct RNA sequencing and newer methods such as 3P-Seq.

PAPERCLIP Provides Comprehensive and Precise mRNA Polyadenylation Maps in Cultured Cells

We next used the PAPERCLIP data to establish an mRNA polyadenylation map in HeLa cells. From two independent replicates (Figure S1A), we identified 17,652 high-confidence poly(A) sites located in 11,785 genes (Figure 2A). Importantly, PAPERCLIP was highly reproducible, as evidenced by the high correlation

resolution to identify exact mRNA 3' ends (Miura et al., 2014), we reasoned that it might provide additional support for 3' UTR extensions identified by PAPERCLIP and broaden the scope of our validation in a high-throughput fashion. Indeed, through RNA-seq, we identified 17 genes that had 100% base coverage in the extended 3' UTRs annotated by PAPERCLIP and an additional 61 genes with more than 90% coverage (Figure S2A; Table S2). Because most of the predicted mRNA transcripts with shortened 3' UTRs also have overlapping longer isoforms, it is difficult to unequivocally demonstrate 3' UTR shortening by RNA-seq alone given its limited power to resolve transcript isoforms. Nevertheless, we were able to confirm several examples of previously unrecognized short 3' UTR isoforms predicted by PAPERCLIP in RNA-seq profiles (Figure S2B). As independent confirmation of the single nucleotide resolution of PAPERCLIP sites, we directly mapped selected individual polyadenylation events by 3' rapid amplification of cDNA ends (RACE) (Figure S2C). In all cases, the exact location of PAPERCLIP sites was validated. Overall, our validation data from northern blot,

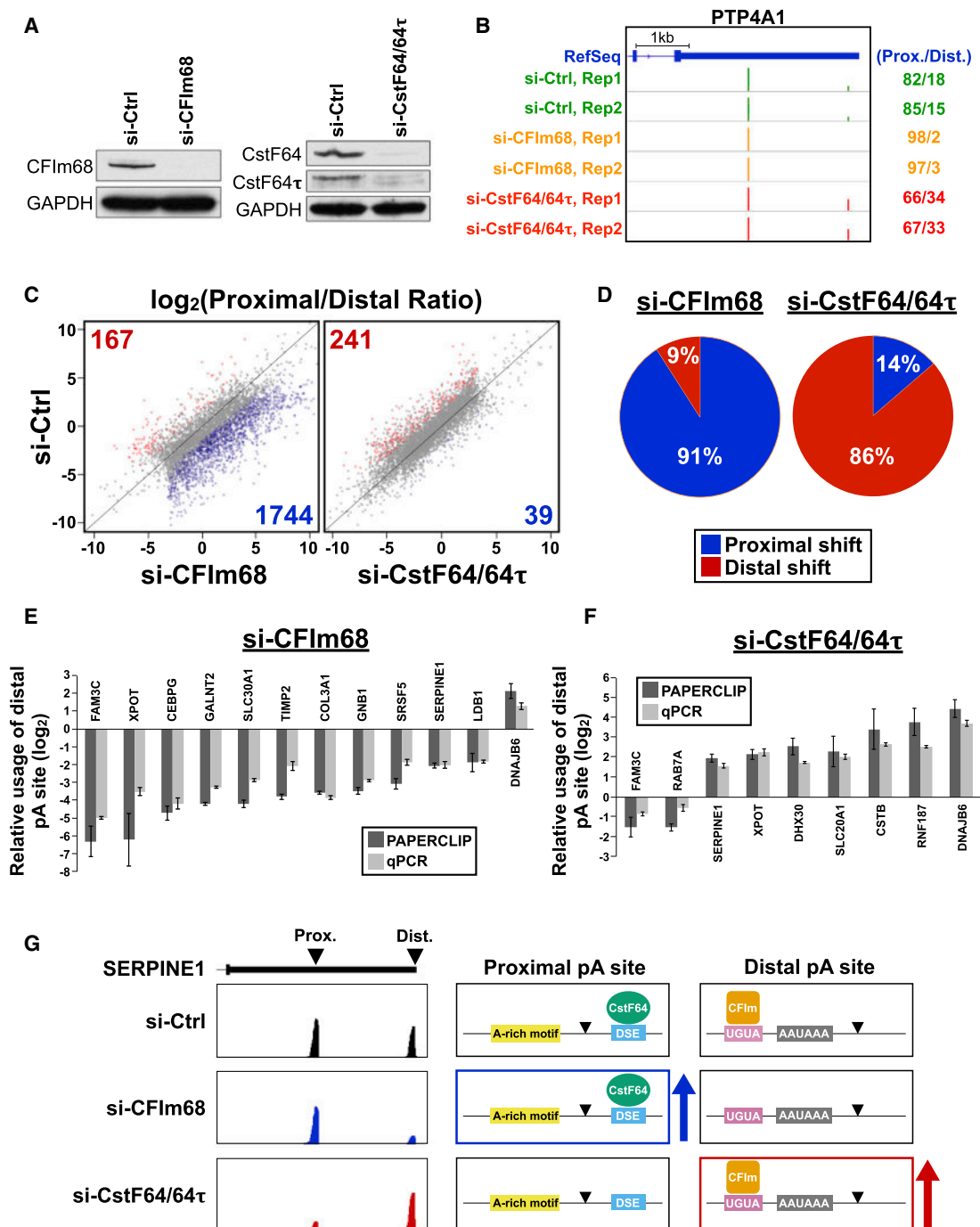


Figure 3. PAPERCLIP Discovers a Role of CstF64/64tau in Promoting Non-canonical Poly(A) Site Usage

(A) Western blots demonstrating siRNA knockdown of CFIm68 and CstF64/64tau in HeLa cells. Ctrl, control.

(B) Diagram showing APA shifts in individual PAPERCLIP experiments following siRNA transfection. Relative peak heights from PAPERCLIP at the proximal and distal poly(A) sites are shown as percentage of the sum of both peaks on the right. Rep, replicate.

(C) Scatterplots comparing $\log_2(\text{proximal/distal [P/D] ratio})$ by PAPERCLIP for two-peak genes between control siRNAs and treatment siRNAs (si-CFIm68 and si-CstF64/64tau). Each dot represents a gene. Genes with a false discovery rate (FDR) < 0.05 and at least a 2-fold change of P/D ratio are considered significantly shifted and are colored. Red, $\log_2[(\text{treatment siRNA P/D ratio})/(\text{control siRNA P/D ratio})] \geq 1$. Blue, $\log_2[(\text{treatment siRNA P/D ratio})/(\text{control siRNA P/D ratio})] \leq -1$. Total numbers of significantly shifted genes for both directions are listed at the corners of the plots.

(D) Pie charts summarizing the direction of APA shift in significantly shifted genes from (C).

(E and F) Diagrams comparing the PAPERCLIP results from (C) and validating the qRT-PCR experiments for individual genes. Error bars represent SE.

(legend continued on next page)

RNA-seq, and 3' RACE provide strong support for the high-resolution mRNA polyadenylation map established by PAPERCLIP in HeLa cells.

To test whether the observations in HeLa cells are generalizable, we performed PAPERCLIP in another cell line, HEK293. Indeed, in HEK293 cells, we were able to obtain 16,414 high-confidence poly(A) sites in 11,488 genes with similarly high reproducibility and specificity for the 3' ends (Figures S1D–S1H). As in HeLa cells, more than half of the annotated genes (6,312, 55%) in HEK293 cells have at least one poly(A) site that is not present in the RefSeq annotation. Altogether, PAPERCLIP has identified 21,040 non-redundant poly(A) sites from HeLa and HEK293 cells. About 32% (6,778 of 21,040) of these poly(A) sites are not present in existing annotations (RefSeq and GENCODE, release 19). Of these un-annotated sites, 4,374 overlap with 3P-Seq read clusters (Nam et al., 2014) and 2,404 (35%) do not. Overall, 89% of the identified poly(A) sites are supported by either the standard annotations or 3P-Seq. Our results suggest that the mRNA polyadenylation events in individual cell lines are incompletely covered by standard annotations, and PAPERCLIP provides a robust tool to establish individualized mRNA polyadenylation maps with high precision and great depth.

PAPERCLIP Offers Transcriptome-wide Assessment of APA in a Quantitative Manner

An important application for mRNA 3' end mapping methods is to identify changes in poly(A) site usage. The mammalian mRNA 3' processing complex contains a large number of proteins, including 15 core factors such as CstF64 and CFIm68 (Shi et al., 2009). Recently, Yao et al. (2012) showed that co-depletion of CstF64 and its paralog CstF64tau in HeLa cells caused 201 genes to shift poly(A) site preference with a bias for the distal poly(A) site. In contrast, Martin et al. (2012) demonstrated that knockdown of CFIm68 in general induced the use of proximal poly(A) sites in HEK293 cells, although the numbers of genes that exhibited a shift in APA preference were not discussed.

To examine the capacity of PAPERCLIP to identify shifts in poly(A) site usage, we performed small interfering RNA (siRNA)-mediated knockdown for CFIm68 and CstF64/64tau in HeLa cells. Western blots demonstrated strong depletion of CFIm68 and CstF64/64tau in cells transfected with the corresponding siRNAs compared with control siRNAs (Figure 3A). We next performed PAPERCLIP to measure poly(A) site usage for all three conditions (Figure 3B). Both siRNA treatments resulted in a large number of APA shifts (1,911 genes in si-CFIm68 and 280 genes in si-CstF64/64tau) compared with control siRNAs (Figure 3C; Table S3). Consistent with previous reports (Martin et al., 2012; Yao et al., 2012), CFIm68 depletion and CstF64/64tau depletion had opposite effects on poly(A) site selection. The former caused a strong shift toward the proximal sites, whereas the latter resulted in a preference for distal sites (Figure 3D). We next performed qRT-PCR as an indepen-

dent measure to evaluate changes in APA under both conditions. In all cases, APA shifts identified by PAPERCLIP were also confirmed by qRT-PCR (Figures 3E and 3F). Although depletion of CFIm68 and CstF64/64tau overall had opposite effects on APA, we observed diverse effects for individual genes. For example, *DNAJB6* preferred the distal site under both conditions, whereas *FAM3C* consistently shifted proximally (Figures 3E and 3F). A recent study identified genes that underwent 3' UTR shortening after CFIm25 knockdown in HeLa cells (Masamha et al., 2014), and we found a strong agreement between the study and our data from CFIm68 depletion (525 of 538, 98%). This result is consistent with current knowledge that both CFIm25 and CFIm68 are part of the CFIm complex (Shi et al., 2009). We conclude that PAPERCLIP is able to offer a transcriptome-wide assessment on APA in a quantitative manner.

PAPERCLIP Discovers a Role of CstF64/64tau in Promoting Non-canonical Poly(A) Site Usage

The binding motifs of the CFIm complex and CstF64/64tau have been characterized. The CFIm complex binds the UGUA motif upstream of the poly(A) sites, whereas CstF64/64tau binds the downstream element (DSE) consisting of U/GU-rich motifs within 30 nt 3' to the poly(A) sites (Martin et al., 2012; Tian and Manley, 2013). Binding of the CFIm complex and CstF64/64tau generally promotes usage of the poly(A) site. Moreover, for certain poly(A) sites that lack A(A/U)UAAA, the canonical poly(A) signal, the UGUA motif or the DSE becomes necessary for their usage (Nunes et al., 2010; Venkataraman et al., 2005). To identify sequence motifs that correlate with regulated APA, we performed an unbiased motif search for all possible 4-mers and 6-mers in proximity to APA sites identified in CFIm68 and CstF64/64tau depletion experiments.

For the 1744 genes showing loss of distal poly(A) site usage upon CFIm68 knockdown, there was a strong enrichment of UGUA (the top enriched 4-mer) and AAUAAA (the top enriched 6-mer) upstream the distal poly(A) site and an enrichment of U/GU-rich motifs (all top ten enriched 6-mers) downstream (Table S3). These results are consistent with current knowledge that the distal poly(A) sites usually contain more canonical sequence elements (Shi, 2012) and explain the loss of distal poly(A) site usage upon depletion of CFIm68.

Interestingly, a different picture emerged from transcripts affected by CstF64/64tau depletion, which shifted predominantly from proximal to distal site usage. For the 241 genes showing loss of proximal poly(A) site usage upon depletion of CstF64/64tau, the proximal poly(A) sites have very strong enrichment of adenine-rich elements (defined as a hexamer with ≥ 5 adenosines excluding AAUAAA [Nunes et al., 2010]; the top four enriched 6-mers) in the upstream region and also enrichment of U/GU-rich elements downstream (eight of the top ten enriched 6-mers) (Table S3). It has been shown that the presence of an adenine-rich sequence and a strong DSE is sufficient to be recognized by the mRNA

(G) Diagrams summarizing the sequence motifs correlated with APA in HeLa cells. SERPINE1 serves as an example. Left: diagrams showing the last exon of SERPINE1, the location of proximal and distal poly(A) sites, and PAPERCLIP read clusters under three experimental conditions. Center and right: diagrams showing the sequence motifs present in the flanking regions of SERPINE1 proximal and distal poly(A) sites in addition to the postulated interactions between them and CstF64/CFIm68. Black triangles denote the poly(A) sites. Arrows denote the increase in poly(A) site usage.

EN2 is another GUKKU-containing gene that also requires both CFlm68 and CstF64/64tau for usage of its two main poly(A) sites (Figure S4A; Figure 4B, top).

The G/U-rich nature of the GUKKU motif suggests that it is part of the DSE and might be involved in poly(A) site selection. To investigate whether the GUKKU motif is simply a sequence element associated with CstF64/64tau-dependent non-canonical poly(A) sites or whether it actually contributes to the usage of these sites, we took advantage of the absence of endogenous EN2 expression in HeLa cells (Figure 4B, bottom) and made a construct expressing GFP upstream of the entire EN2 3' UTR (pEN2, Figure 4C). pEN2 faithfully recapitulates the APA pattern observed in endogenous EN2 in LN229 when transfected into HeLa cells (Figure S4B) and exhibits APA shifts upon CFlm68 or CstF64/64tau depletion (Figure S4C). It was previously shown that adenine-rich elements are important for non-canonical poly(A) site recognition (Nunes et al., 2010). Therefore, we generated pEN2 mutants with mutated GUKKU motifs or adenine-rich elements (Figure 4D) and examined their APA patterns by PAPERCLIP. Indeed, both mutants had decreased proximal poly(A) site usage (Figures 4E and 4F), suggesting that both elements participate in proximal poly(A) site selection and are necessary for its full usage.

To further test the functionality of the GUKKU motif, we performed additional experiments using the pEN2 construct as a tool. We identified a non-canonical poly(A) site in NOTCH1 that did not contain downstream GU-rich elements or exhibited a shift upon CstF64/64tau depletion (NOTCH1-WT, Figure S4D). Therefore, we generated a hybrid poly(A) site in which the upstream half sequence originates from the NOTCH1 poly(A) site and the downstream half sequence (containing the GUKKU motifs) comes from the EN2 proximal poly(A) site (NOTCH1-HYB, Figure S4D). We also generated a mutant version of NOTCH1-HYB in which mutations were introduced to the GUKKU motifs (NOTCH1-MUT, Figure S4D). We then made three new constructs in which the pEN2 proximal poly(A) site was replaced by each of the aforementioned NOTCH1 sites and confirmed their usage by 3' RACE (data not shown). qPCR experiments demonstrated a sensitivity to CstF64/64tau depletion for NOTCH1-HYB, which was completely abolished in NOTCH1-MUT (Figure S4E). Together, these results provide further support for a functional role of the GUKKU motif in the selection of a non-canonical poly(A) site by CstF64/64tau.

We next wished to determine whether other GUKKU-containing non-canonical poly(A) sites that are not part of the 58-gene list could substitute functionally for the EN2 proximal poly(A) site and exhibit CstF64/64tau dependence. We searched for candidate poly(A) sites in a group of genes that used only one poly(A) site throughout the siRNA experiments and therefore were not included in the APA shift analysis (Figure S4F). We identified two non-canonical poly(A) sites in SRSF9 and JUNB that contain an upstream adenine-rich element and downstream GUKKU motifs but otherwise do not resemble the EN2 proximal poly(A) site in sequence. Therefore, we made new pEN2 hybrid constructs in which the EN2 proximal poly(A) site was replaced with the SRSF9 or JUNB poly(A) site (Figure 4G). Usage of the inserted poly(A) sites was confirmed by 3' RACE (data not shown). Indeed, upon CstF64/64tau depletion, both constructs showed a

distal shift similar to EN2 (Figure 4H), suggesting that CstF64/64tau also promotes usage of the two poly(A) sites in pEN2. Moreover, these results also indicate that SRSF9 and JUNB might have non-permissive sequence context that prevents an APA shift. To test the hypothesis that the lack of a second functional poly(A) site might contribute to the absence of an APA shift in JUNB, we generated pAcGFP-JUNB by cloning the entire JUNB 3' UTR plus ~100 bp sequence 3' to the JUNB poly(A) site into pAcGFP-C1, which contains a poly(A) site downstream of the cloning site (Figure S4G). Interestingly, CstF64/64tau depletion resulted in a strong distal APA shift for pAcGFP-JUNB (Figure S4H), providing evidence that the surrounding sequence context indeed contributes to poly(A) site usage. Taken together, these results demonstrate that PAPERCLIP is able to identify a functional sequence motif that participates in poly(A) site selection de novo and provide insights into APA regulation.

PAPERCLIP Identifies Unannotated 3' UTR Extensions that Have Regulatory Functions in the Mouse Brain

Neurons use multiple neuron-specific RBPs and miRNAs to regulate mRNA metabolism (Darnell, 2013). It is well documented that brain mRNAs as a group have the longest 3' UTRs compared with mRNAs in other tissues (Ji et al., 2009; Lianoglou et al., 2013; Ulitsky et al., 2012). Many mRNAs have neuron-specific 3' UTR extensions that may provide platforms to interact with RBPs and miRNAs (Hilgers et al., 2011; Smibert et al., 2012). To identify 3' UTR regulatory elements in the brain, we first performed PAPERCLIP in the adult mouse cortex and annotated 10,117 poly(A) sites from 8,354 genes (Figures S5A–S5C). Overall, PAPERCLIP identified 1,024 3' UTR extensions that were not present in the RefSeq annotation (Figure S5D; Table S5). Miura et al. (2013) recently identified many 3' UTR extensions in the mouse brain through RNA-seq analysis. Therefore, we further compared the identified 3' UTR extensions with GENCODE annotation and the 3' UTR extensions reported by Miura et al. (2013). In more than half of the cases (566 of 1,024, 55%), the distal poly(A) sites identified by PAPERCLIP that demarcate the 3' UTR extensions do not overlap with either GENCODE M2 annotation or the 3' ends of the 3' UTR extensions reported by Miura et al. (2013). To provide support for the presence of the 566 3' UTR isoforms identified by PAPERCLIP, we performed RNA-seq and examined the extended 3' UTRs for mapped reads. 457 (81%) PAPERCLIP-identified 3' UTR extensions have FPKM ≥ 1 and 351 (62%) have RNA-seq coverage at above 90% (129 have 100% coverage), providing strong support for the annotation by PAPERCLIP. Taken together, these results further expand the list of 3' UTR extensions in the mouse brain and demonstrate the capacity of PAPERCLIP to provide comprehensive poly(A) site maps for complex living tissues.

To identify regulatory elements located in the 1,024 extended 3' UTRs identified by PAPERCLIP, we overlaid Ago HITS-CLIP data from the mouse cortex and searched for miRNA seed matches in Ago footprints located in the extended 3' UTRs. To make sure that the identified regulatory relationship occurs in the same cell type, we examined miR-128, a miRNA that is highly enriched in the brain and exhibits a neuron-specific expression pattern (Bruno et al., 2011). We identified 48 miR-128 seed matches overlapping robust Ago binding sites in the extended

3' UTRs and selected eight neuronal transcripts to test the functionality of the predicted miR-128 binding sites by luciferase assay (Table S5). In all cases, the repression of luciferase reporter expression was dependent on the presence of a miR-128 mimic and the wild-type miR-128 binding site (Figure 5A), suggesting that these sites are indeed functional. In a recent study, Tan et al. (2013) identified 154 miR-128 targets in mouse D1-neurons by combining FLAG-Ago2 HITS-CLIP and ribosome-associated mRNA analysis. We hypothesized that the newly identified miR-128 sites in the 3' UTR extension might allow us to find additional miR-128 targets using the mRNA expression dataset generated by Tan et al. (2013). Indeed, we identified five genes that are not on the Tan et al. (2013) gene list and have increased ribosome association in miR-128-deficient D1 neurons, including three genes that we validated in luciferase assays (Figures 5B and 5C). The increase in ribosome association of the five miR-128 targets identified in this study is similar to the previously identified 154 genes (Figure 5D; $p = 0.37$, Wilcoxon rank-sum test). These results indicate that functional regulatory sequences might currently be overlooked because of incomplete coverage of mRNA 3' end annotations and that PAPERCLIP can identify 3' UTR extensions that mediate regulatory functions.

PAPERCLIP Uncovers an Evolutionarily Conserved APA Shift during Brain Development

Last, to investigate whether APA occurs during mouse brain development, we performed PAPERCLIP in the embryonic mouse cortex (Figures S5E–S5G) and compared the relative usage of poly(A) sites between adult and embryonic mouse cortex. PAPERCLIP identified 444 genes that significantly changed poly(A) site usage (Figure 6A; Table S6). Follow-up qRT-PCR experiments validated the PAPERCLIP results (Figures 6B and 6C).

A very recent RNA-seq study using human cortex samples identified many differentially expressed regions (DERs) in the human genome across six life stages from fetus to middle age (Jaffe et al., 2015). Although RNA-seq does not detect APA shifts with high sensitivity, we decided to explore the possibility that some of the APA shifts identified by PAPERCLIP could also be detected in humans by comparing our data with the reported DERs. We first lifted the coordinates of both the proximal and distal mouse poly(A) sites from the 444 genes to the human genome and then compared the regions flanked by the lifted poly(A) sites to the DERs. This analysis identified three candidate genes (*DCX*, *XPR1*, and *ATP2B2*) in which the regions flanked by the lifted mouse poly(A) sites have >80% coverage by DERs. To exclude the possibility that the observed differential expression in Jaffe et al. (2015) was due to transcriptional changes, we calculated the overlap between DERs and all exons for each gene. The overlap between DERs and all exons in *ATP2B2* was 26% because only the last exon contains DERs (Figure 6D). In contrast, *DCX* and *XPR1* have almost perfect overlap between DERs and all of their exons (>98%), suggesting that the major source for differential expression is transcription instead of alternative usage of the 3' UTR sequence. Therefore, we excluded *DCX* and *XPR1* from further analysis.

In mouse *Atp2b2*, PAPERCLIP identified an increased usage of the distal 3' UTR sequence in the adult (Figure 6E). Interest-

ingly, the mouse distal poly(A) site identified by PAPERCLIP actually corresponds to the annotated poly(A) site in humans, suggesting that the mouse annotation is incomplete (Figure 6D). To examine whether usage of the distal 3' UTR sequence is also increased in adult humans, we mapped the RNA-seq raw reads from Jaffe et al. (2015) and compared the distal 3' UTR-to-proximal 3' UTR read count ratio between fetus and adult. This analysis indeed revealed a significant increase in distal 3' UTR usage in the human adult (Fisher's exact test, $p < 0.01$) (Figure 6E).

To identify regulatory elements located in the mouse *Atp2b2* distal 3' UTR, we again overlaid the Ago HITS-CLIP data to search for miRNA seed matches in Ago footprints located in the distal 3' UTR. MicroRNAs that have additional seed matches in the proximal 3' UTR or upstream exons were excluded from further analysis. We identified a conserved miR-137 binding site near the end of the human *ATP2B2* distal 3' UTR (Figures 6D and 6F). The finding is highly intriguing because both *Atp2b2* and miR-137 are mainly expressed in neurons (Smrt et al., 2010; Strehler and Zacharias, 2001), and miR-137 is known to play roles in neuronal development (Meza-Sosa et al., 2014) and human hearing (Schultz et al., 2005). Therefore, we performed a luciferase assay in HEK293 cells to examine the functionality of the identified miR-137 binding site, which resulted in repression similar in magnitude to that of a previously validated miR-137 binding site in *Mib1* (Smrt et al., 2010; Figure 6G). Taken together, these results demonstrate that PAPERCLIP is able to provide critical information to guide the discovery of evolutionarily conserved APA shifts and uncover regulatory relationships between mRNAs and miRNAs.

DISCUSSION

In this study, we describe PAPERCLIP, an mRNA 3' end mapping method based on the CLIP technique. In contrast to the original HITS-CLIP (Licatalosi et al., 2008), which aims to identify transcriptome-wide binding sites of the protein of interest, PAPERCLIP uses PABP as a tool to specifically retrieve mRNA fragments containing 3' UTR sequences immediately upstream of the poly(A) sites. This use of a robust biological filter for poly(A) sites distinguishes PAPERCLIP from other mRNA 3' end mapping methods that require in silico filtering or sophisticated molecular biology techniques to achieve selection against an internal adenine-rich sequence. We provide evidence that PAPERCLIP has an excellent signal-to-noise ratio, ameliorates the internal priming problem commonly seen in 3' end sequencing, and compares favorably with many other mRNA 3' end mapping methods. We further demonstrate the capacity of PAPERCLIP in two major applications for mRNA 3' end mapping methods: detecting APA shifts and discovering 3' UTR-mediated mRNA regulation.

By combining PAPERCLIP and siRNA knockdown in two cell lines, we provided a comprehensive list of genes that exhibited APA shifts upon CFIm68 or CstF64/64tau depletion. In line with recent studies (Martin et al., 2012; Yao et al., 2012, 2013), our results suggest that CstF64 and CstF64tau, originally considered "general" mRNA 3' end-processing factors, only contribute to a subset of poly(A) site selections. Additionally, we discovered a previously unrecognized role of CstF64/64tau in promoting the

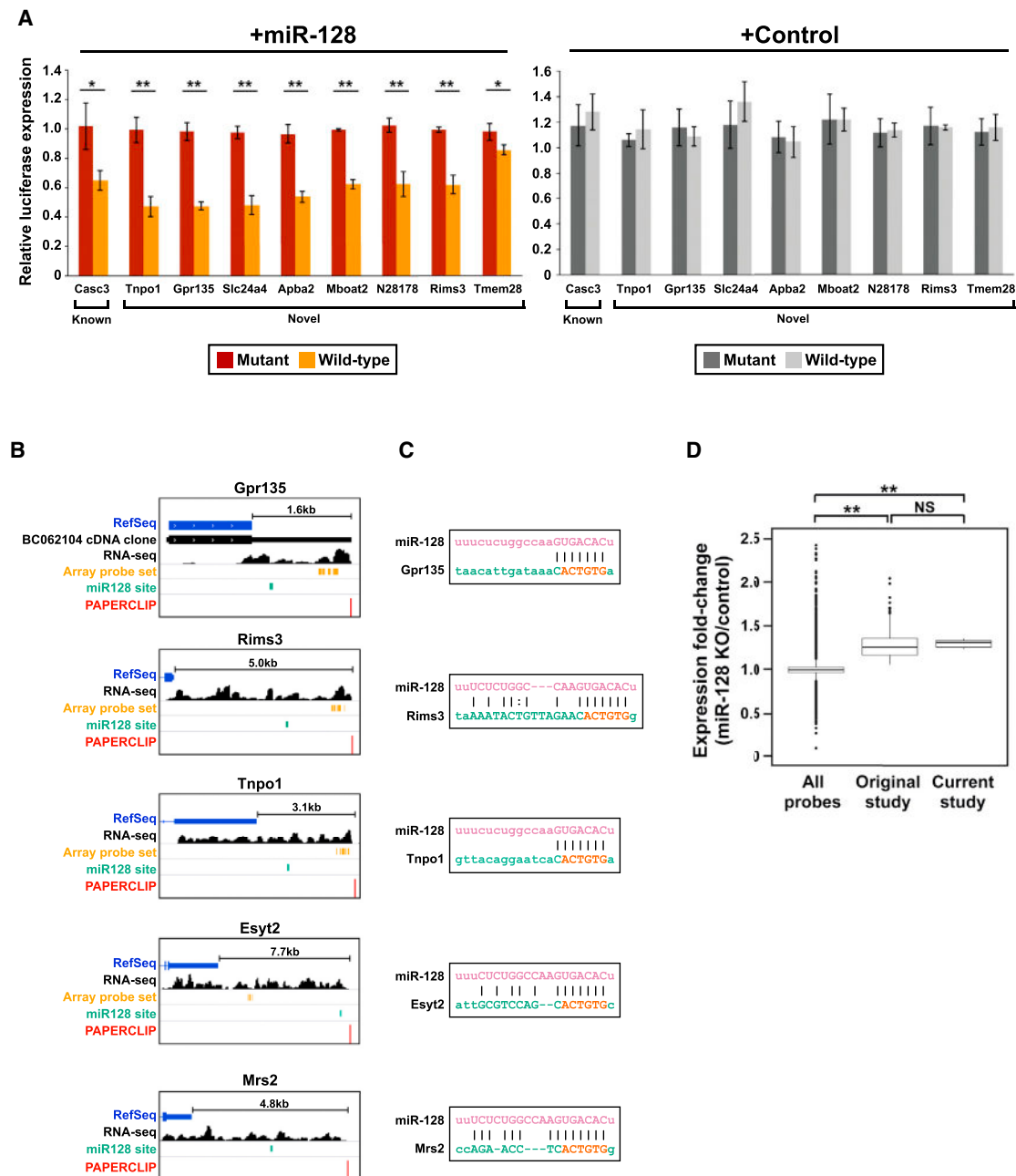


Figure 5. PAPERCLIP Identifies Additional miR-128 Targets

(A) Results of the luciferase assay experiments in HEK293 cells co-transfected with miR-128 mimic (left) and control mimic (right) (n = 3). Error bars represent SD. *p < 0.05, **p < 0.01. The differences between the mutant and wild-type for all constructs in the control mimic experiment were not statistically significant.

(B) Diagrams showing RefSeq annotation, RNA-seq, and PAPERCLIP results in addition to the locations of miR-128 binding site and the microarray probe set for the five miR-128 targets identified in this study. The peak heights from PAPERCLIP are scaled for each gene. The bar above the RefSeq annotation indicates the length of the 3' UTR extension. For Gpr135, the poly(A) site identified by PAPERCLIP is at the 3' end of a full-length cDNA clone, BC062104, which is included in the diagram. The microarray probe set for Mrs2 is located 5' to the last exon and therefore is not shown. For all five genes, no other miR-128 binding sites were found outside of the regions shown.

(C) Diagrams showing the pairing between miR-128 and the five targets shown in (B) as determined by the miRanda algorithm. The miR-128 sequence is shown from 3' to 5', and the target sequence is shown from 5' to 3'. The miR-128 seed sequence is shown in red.

(D) Box plots showing the increased ribosome association of five additional miR-128 targets (Current study) in miR-128 deficient D1 neurons. All probes in the same dataset (All probes) and the 154 miR-128 target genes identified in the original study (Original study) (Tan et al., 2013) are shown for comparison. Six outliers in the "All probes" group are not shown. **p < 0.01. NS, not significant.

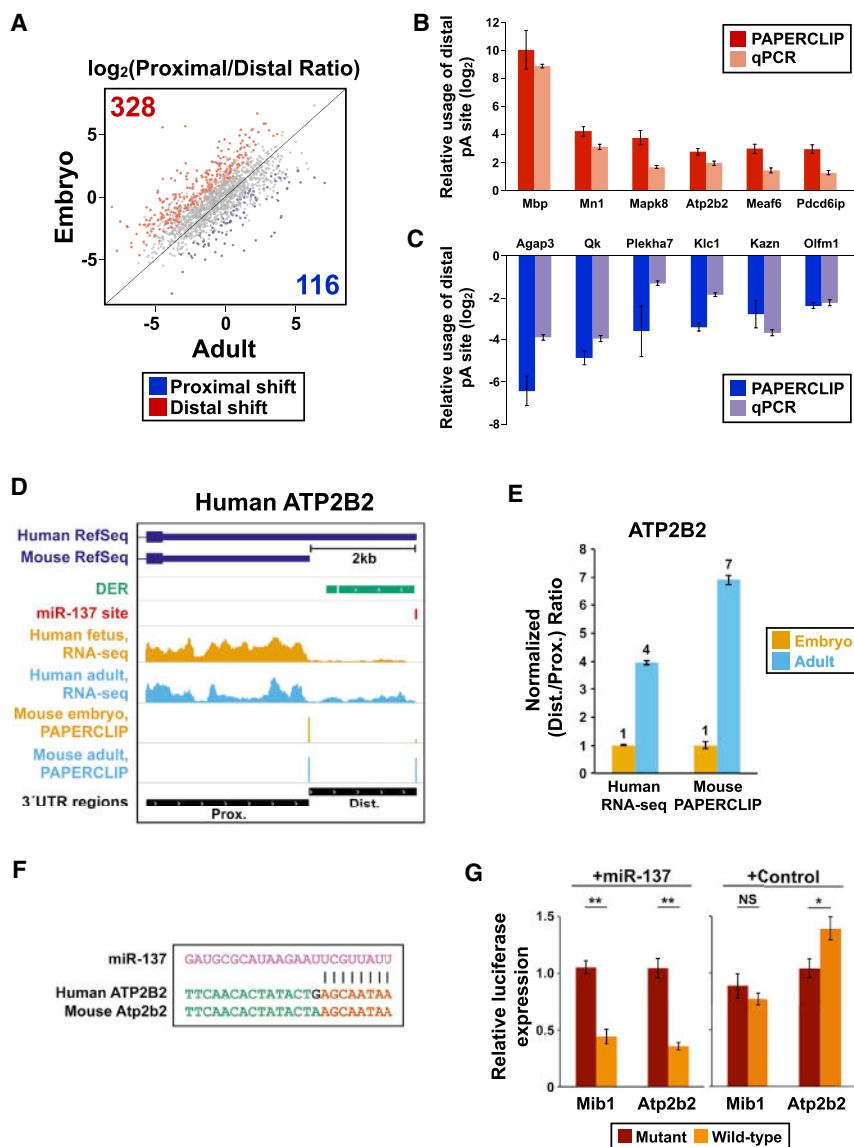


Figure 6. PAPERCLIP Identifies an Evolutionarily Conserved APA Shift during Brain Development

(A) Scatterplots comparing $\log_2(\text{proximal/distal ratio})$ by PAPERCLIP for two-peak genes between the embryo and adult mouse cortex. Each dot represents a gene. Genes with $\text{FDR} < 0.05$ and at least a 2-fold change of P/D ratio are considered significantly shifted and are colored. Red, $\log_2[(\text{embryo P/D ratio})/(\text{adult P/D ratio})] \geq 1$. Blue, $\log_2[(\text{embryo P/D ratio})/(\text{adult P/D ratio})] \leq -1$. Total numbers of significantly shifted genes for both directions are listed at the corners of the plots. (B and C) Diagrams comparing the PAPERCLIP results from (A) and validating qRT-PCR experiments for individual genes. Error bars represent SE. (D) Diagrams showing both human and mouse RefSeq annotation, the locations of DERs and the miR-137 site, human RNA-seq results from Jaffe et al. (2015), and the mouse PAPERCLIP results for human *ATP2B2*. The mouse RefSeq annotation and PAPERCLIP results were lifted from mm10 to hg19.

(E) Bar graph showing the relative usage of the distal 3' UTR in the *ATP2B2* gene for both human and mouse. The mouse PAPERCLIP results were re-plotted from (B) for comparison. Error bars represent SE.

(F) Diagrams showing the pairing between miR-137 and the target site in the *ATP2B2* gene in both human and mouse. The miR-128 sequence is shown from 3' to 5', and the target sequence is shown from 5' to 3'. The miR-137 seed sequence is shown in red.

(G) Results of the luciferase assay experiments in HEK293 cells co-transfected with miR-137 mimic (left) and control mimic (right) ($n = 3$). Error bars represent SD. * $p < 0.05$, ** $p < 0.01$.

usage of non-canonical poly(A) sites. We further identified a GUKKU motif that is enriched in these CstF64/64tau-sensitive non-canonical poly(A) sites and established its direct role in promoting poly(A) site usage. It is well established that human CstF64 and CstF64tau favors G/U-rich sequences for interaction (Takagaki and Manley, 1997; Yao et al., 2013). We believe that the GUKKU motif likely represents one of many naturally occurring motifs in DSEs or CstF64/64tau-interaction sequences, which is supported by its presence in some well-known canonical poly(A) sites (Figure S6A). We do not exclude the possibility that additional sequence elements in the 58 non-canonical poly(A) sites might also participate in their selection, and future studies will be necessary to fully characterize their DSEs, which will be greatly facilitated by the pEN2 construct described in this study.

The advantages of PAPERCLIP are further illustrated in our studies using brain, which harbors many long 3' UTR extensions

Moreover, PAPERCLIP identified additional miR-128 targets in the adult mouse cortex and discovered a regulatory relationship between miR-137 and *Atp2b2* during mouse cortex development. It is known that miRNA binding sites tend to locate near alternative and constitutive polyadenylation sites (Grimson et al., 2007). Indeed, we found a strong enrichment of miRNA binding sites upstream of PAPERCLIP-identified poly(A) sites in the adult mouse cortex (Figure S6B), which further supports the strength of PAPERCLIP.

Recent studies in *Drosophila* revealed the presence of a tissue-specific gene regulatory network consisting of neuron-specific miRNAs and neural 3' UTR extensions in the adult brain (Figure S6C; Hilgers et al., 2011; Smibert et al., 2012). Interestingly, an examination of publicly available RNA-seq data (ENCODE Project Consortium, 2012) showed that the main APA isoform of *ATP2B2/Atp2b2* in both the human and mouse adult liver is

also the proximal form (Figure S6D; data not shown). Therefore, although further studies are necessary to fully elucidate the functional significance of the potential regulation between *Atp2b2* and miR-137 in the adult brain, our results provide an example of mammalian neural 3' UTR extension that is both tissue-specific and developmentally controlled.

The identification of an APA shift during mouse brain development by PAPERCLIP also provided an opportunity to examine whether APA affects gene expression in this context. We found that single poly(A) site genes as a group were enriched in the differentially expressed genes between the embryo and adult brain (Figure S6E). In addition, we also found that the overlap between multi-poly(A) site genes that changed abundance and multi-poly(A) site genes that exhibited an APA shift was not higher than what would be expected by chance (Figure S6F). These two findings are consistent with a recent work from Lianoglou et al. (2013) in which they discovered that an APA shift and changes in mRNA abundance are largely separate processes in two models of cellular transformation. Nevertheless, we do not rule out the possibility that a link between APA and gene expression is present in certain cell type(s) that is not detectable at the whole cortex level.

Extending insights into post-transcriptional regulation in vivo, particularly brain, is vastly complicated by the coexistence of multiple cell types that have distinct functions. It has been shown that a subset of neuronal genes exhibit 3' UTR extension during development in *Drosophila* (Hilgers et al., 2011; Smibert et al., 2012). It remains unclear whether an increase in the use of the distal 3' UTR during development is limited to neurons or whether it is a general property for all major cell types in the brain. Using data from a recent cell-type-specific RNA-seq study (Zhang et al., 2014), we identified 84 cell-type-enriched genes from our list of 444 genes that significantly changed poly(A) site usage between embryos and adults (Table S6). Interestingly, although neuron-enriched genes are the largest class (39 of 84, 46%, including *Atp2b2*), five major brain cell types (astrocytes, neurons, oligodendrocytes, microglia, and endothelial cells) have at least one gene that exhibits an APA shift, suggesting that APA shifts occur in more than one cell type during mouse brain development (Zhang et al., 2014). It is therefore increasingly clear that cell-type-specific poly(A) site maps will be necessary to understand how individual cell types regulate APA during brain development. A key feature that distinguishes PAPERCLIP from other mRNA 3' end mapping methods is the potential to modify the target cell population by restricting PABP expression. Because technologies to achieve cell-type-specific control of transgene expression in vivo are readily available (Utomo et al., 1999), PAPERCLIP is uniquely suited for the development of cell-type-specific mRNA 3' end mapping compared with other methods that require prior isolation of pure cell types to establish cell type specificity, a process that is laborious and may introduce bias such as stress signals (Okaty et al., 2011).

EXPERIMENTAL PROCEDURES

Statistical Methods

Wilcoxon rank-sum test, Fisher's exact test, hypergeometric test, and Student's t test were performed using R or Excel. For APA shift, EdgeR package

(Robinson et al., 2010) was used to statistically test significant APA shifts between two experimental conditions while accounting for biological and technical variability between experimental replicates.

PAPERCLIP

Sample preparation, immunoprecipitation, SDS-PAGE, and RNA extraction were adapted from standard HITS-CLIP (Moore et al., 2014). Mouse monoclonal anti-PABP (Sigma, P6246) was used for immunoprecipitation. The sequencing library was constructed using the bromodeoxyuridine (BrdU)-CLIP method (Weyn-Vanhenryck et al., 2014) with modifications to improve sensitivity. The library contains a 14-nt degenerate linker sequence at the 5' end (6-nt random bar code followed by an 8-nt sample multiplexing index) or an 11-nt degenerate linker sequence at the 5' end (3-nt degenerate sequence, 4-nt sample multiplexing index, and 7-nt random bar code). The complete protocol is detailed in the Supplemental Protocol. To minimize batch effects, the entire process was performed independently for replicate experiments, sometimes using primers with different indices. Individual PAPERCLIP libraries were multiplexed and sequenced by HiSeq 2000 or MiSeq (Illumina) to obtain 100-nt (HiSeq) or 75-nt (MiSeq) single-end reads.

Comparison with Other 3' End Mapping Methods

For Figures 1E and 1F, raw reads were downloaded from the NCBI Sequence Read Archive (SRR568012, SRR1033820, SRR299108, SRR090236, SRR453410, and SRR317197) and processed before mapping to hg19 (Novoalign, same settings as for PAPERCLIP). When necessary, the poly(A) sequence at the 3' end was trimmed using CutAdapt. For 3P-Seq and 3' Seq, two methods that often include untemplated adenines in the sequencing reads, only trimmed reads were used for mapping. For all libraries, only uniquely mapped reads were used for analysis. Downstream adenine-rich reads were defined as in the literature (Derti et al., 2012; Shepard et al., 2011): reads that have six consecutive adenines or at least seven adenines total in the ten nucleotides immediately downstream of the last aligned position in the human genome. Reference BED files were downloaded from the University of California, Santa Cruz (UCSC) genome browser for annotating the genomic localization of mapped reads.

Northern Blots

Total RNA from HeLa cells was prepared by Trizol (Invitrogen) extraction and column purification using the High Pure RNA isolation kit (Roche). 10 μ g total RNA per lane was separated with 0.8% SeaKem Gold agarose (Lonza) along with Millennium RNA markers (Ambion). The gel was treated with 0.05 M NaOH, 1.5 M NaCl for 20 min and then with 0.5 M Tris (pH 7.5), 1.5 M NaCl for 10 min before being equilibrated for blotting in 20 \times saline sodium citrate (SSC) for 20 min. The gel was blotted onto a Hybond-N filter (Amersham). Probes were prepared using the Prime-It II random primer labeling kit (Agilent) with [α -³²P] deoxycytidine triphosphate (dCTP). All primer sequences are listed in Table S1. For hybridization, labeled probes were used at 1 \times 10⁶ counts per million (cpm)/ml of hybridization solution (1% BSA fraction V, 7% SDS, 0.5 M NaH₂PO₄ [pH 7], and 1 mM EDTA [pH 8]). The filter was hybridized overnight at 68°C and washed with 2 \times SSC, 0.05% SDS at 60°C twice for 10 min and then with 0.1 \times SSC, 0.1% SDS at 60°C twice for 30 min.

SDS-PAGE and Western Blots

20 μ g total protein per lane was separated on 10% Novex NuPAGE Bis-Tris gels (Invitrogen) and transferred to a nitrocellulose membrane following standard procedures. The following antibodies were used for western blotting: rabbit polyclonal anti-CFIm68 (A301-356A, Bethyl Laboratories, 1:1,000), rabbit polyclonal anti-CstF64 (A301-093A, Bethyl Laboratories, 1:1,000), rabbit polyclonal anti-CstF64tau (A301-487A, Bethyl Laboratories, 1:1,000), and mouse monoclonal anti-GAPDH (ab8245, Abcam, 1:2,000).

Animals

Adult (8- to 14-week-old) and pregnant embryonic day 15.5 (E15.5) C57BL/6J mice were obtained from The Jackson Laboratory. Dissection of the adult and embryonic brain cortex was performed following standard procedures. All procedures were conducted according to the Institutional Animal Care and Use Committee (IACUC) guidelines at Rockefeller University.

ACCESSION NUMBERS

The accession number for the PAPERCLIP and RNA-seq data reported in this paper is GEO: GSE66092.

SUPPLEMENTAL INFORMATION

Supplemental Information includes Supplemental Experimental Procedures, six figures, and six tables and can be found with this article online at <http://dx.doi.org/10.1016/j.celrep.2016.03.023>.

AUTHOR CONTRIBUTIONS

H.W.H. and R.B.D. conceived the project. H.W.H. designed the experiments. R.B.D. supervised the project. H.W.H. and A.M. developed the PAPERCLIP protocol. J.J.F. performed the northern blot experiments. Y.S. performed the mouse embryo dissection. H.W.H. performed all other experiments. H.W.H., C.Y.P., and H.G. performed the bioinformatics analyses. M.J.M. provided the Ago HITS-CLIP data. H.W.H. and R.B.D. wrote the manuscript.

ACKNOWLEDGMENTS

We thank Connie Zhao and Christine Lai (Rockefeller University Genomics Resource Center) for their support with high-throughput sequencing. We thank Nathalie Blachere, Jennifer Darnell, Shengdong Ke, Joseph Luna, Claudia Scheckel, and Chaolin Zhang for comments and suggestions. H.W.H. is an HHMI Fellow of the Life Sciences Research Foundation. Y.S. is a JSPS Postdoctoral Fellow for Research Abroad. R.B.D. is an Investigator of the Howard Hughes Medical Institute. This work was also in part supported by grants from the NIH (NS034389 and NS081706) and the Simons Foundation (SFARI 240432 to R.B.D.).

Received: September 29, 2015

Revised: January 11, 2016

Accepted: March 4, 2016

Published: March 31, 2016

REFERENCES

- Bruno, I.G., Karam, R., Huang, L., Bhardwaj, A., Lou, C.H., Shum, E.Y., Song, H.-W., Corbett, M.A., Gifford, W.D., Gecz, J., et al. (2011). Identification of a microRNA that activates gene expression by repressing nonsense-mediated RNA decay. *Mol. Cell* 42, 500–510.
- Chi, S.W., Zang, J.B., Mele, A., and Darnell, R.B. (2009). Argonaute HITS-CLIP decodes microRNA-mRNA interaction maps. *Nature* 460, 479–486.
- Darnell, R.B. (2013). RNA protein interaction in neurons. *Annu. Rev. Neurosci.* 36, 243–270.
- Derti, A., Garrett-Engle, P., Macisaac, K.D., Stevens, R.C., Sriram, S., Chen, R., Rohl, C.A., Johnson, J.M., and Babak, T. (2012). A quantitative atlas of polyadenylation in five mammals. *Genome Res.* 22, 1173–1183.
- Di Giammartino, D.C., Nishida, K., and Manley, J.L. (2011). Mechanisms and consequences of alternative polyadenylation. *Mol. Cell* 43, 853–866.
- Elkon, R., Ugalde, A.P., and Agami, R. (2013). Alternative cleavage and polyadenylation: extent, regulation and function. *Nat. Rev. Genet.* 14, 496–506.
- ENCODE Project Consortium (2012). An integrated encyclopedia of DNA elements in the human genome. *Nature* 489, 57–74.
- Grimson, A., Farh, K.K.-H., Johnston, W.K., Garrett-Engle, P., Lim, L.P., and Bartel, D.P. (2007). MicroRNA targeting specificity in mammals: determinants beyond seed pairing. *Mol. Cell* 27, 91–105.
- Hilgers, V., Perry, M.W., Hendrix, D., Stark, A., Levine, M., and Haley, B. (2011). Neural-specific elongation of 3' UTRs during *Drosophila* development. *Proc. Natl. Acad. Sci. USA* 108, 15864–15869.
- Hoque, M., Ji, Z., Zheng, D., Luo, W., Li, W., You, B., Park, J.Y., Yehia, G., and Tian, B. (2013). Analysis of alternative cleavage and polyadenylation by 3' region extraction and deep sequencing. *Nat. Methods* 10, 133–139.

Jaffe, A.E., Shin, J., Collado-Torres, L., Leek, J.T., Tao, R., Li, C., Gao, Y., Jia, Y., Maher, B.J., Hyde, T.M., et al. (2015). Developmental regulation of human cortex transcription and its clinical relevance at single base resolution. *Nat. Neurosci.* 18, 154–161.

Jenal, M., Elkon, R., Loayza-Puch, F., van Haften, G., Kühn, U., Menzies, F.M., Oude Vrielink, J.A.F., Bos, A.J., Drost, J., Rooijers, K., et al. (2012). The poly(A)-binding protein nuclear 1 suppresses alternative cleavage and polyadenylation sites. *Cell* 149, 538–553.

Ji, Z., Lee, J.Y., Pan, Z., Jiang, B., and Tian, B. (2009). Progressive lengthening of 3' untranslated regions of mRNAs by alternative polyadenylation during mouse embryonic development. *Proc. Natl. Acad. Sci. USA* 106, 7028–7033.

Kahvejian, A., Roy, G., and Sonenberg, N. (2001). The mRNA closed-loop model: the function of PABP and PABP-interacting proteins in mRNA translation. *Cold Spring Harb. Symp. Quant. Biol.* 66, 293–300.

Lianoglou, S., Garg, V., Yang, J.L., Leslie, C.S., and Mayr, C. (2013). Ubiquitously transcribed genes use alternative polyadenylation to achieve tissue-specific expression. *Genes Dev.* 27, 2380–2396.

Licatalosi, D.D., and Darnell, R.B. (2010). RNA processing and its regulation: global insights into biological networks. *Nat. Rev. Genet.* 11, 75–87.

Licatalosi, D.D., Mele, A., Fak, J.J., Ule, J., Kayikci, M., Chi, S.W., Clark, T.A., Schweitzer, A.C., Blume, J.E., Wang, X., et al. (2008). HITS-CLIP yields genome-wide insights into brain alternative RNA processing. *Nature* 456, 464–469.

Martin, G., Gruber, A.R., Keller, W., and Zavolan, M. (2012). Genome-wide analysis of pre-mRNA 3' end processing reveals a decisive role of human cleavage factor I in the regulation of 3' UTR length. *Cell Rep.* 1, 753–763.

Masamha, C.P., Xia, Z., Yang, J., Albrecht, T.R., Li, M., Shyu, A.B., Li, W., and Wagner, E.J. (2014). CFIm25 links alternative polyadenylation to glioblastoma tumour suppression. *Nature* 510, 412–416.

Meza-Sosa, K.F., Pedraza-Alva, G., and Pérez-Martínez, L. (2014). microRNAs: key triggers of neuronal cell fate. *Front. Cell. Neurosci.* 8, 175.

Miura, P., Shenker, S., Andreu-Agullo, C., Westholm, J.O., and Lai, E.C. (2013). Widespread and extensive lengthening of 3' UTRs in the mammalian brain. *Genome Res.* 23, 812–825.

Miura, P., Sanfilippo, P., Shenker, S., and Lai, E.C. (2014). Alternative polyadenylation in the nervous system: to what lengths will 3' UTR extensions take us? *BioEssays* 36, 766–777.

Moore, M.J., Zhang, C., Gantman, E.C., Mele, A., Darnell, J.C., and Darnell, R.B. (2014). Mapping Argonaute and conventional RNA-binding protein interactions with RNA at single-nucleotide resolution using HITS-CLIP and CIMS analysis. *Nat. Protoc.* 9, 263–293.

Nam, D.K., Lee, S., Zhou, G., Cao, X., Wang, C., Clark, T., Chen, J., Rowley, J.D., and Wang, S.M. (2002). Oligo(dT) primer generates a high frequency of truncated cDNAs through internal poly(A) priming during reverse transcription. *Proc. Natl. Acad. Sci. USA* 99, 6152–6156.

Nam, J.-W., Rissland, O.S., Koppstein, D., Abreu-Goodger, C., Jan, C.H., Agarwal, V., Yildirim, M.A., Rodríguez, A., and Bartel, D.P. (2014). Global analyses of the effect of different cellular contexts on microRNA targeting. *Mol. Cell* 53, 1031–1043.

Nunes, N.M., Li, W., Tian, B., and Furger, A. (2010). A functional human Poly(A) site requires only a potent DSE and an A-rich upstream sequence. *EMBO J.* 29, 1523–1536.

Okaty, B.W., Sugino, K., and Nelson, S.B. (2011). A quantitative comparison of cell-type-specific microarray gene expression profiling methods in the mouse brain. *PLoS ONE* 6, e16493.

Ozsolak, F., Kapranov, P., Foissac, S., Kim, S.W., Fishilevich, E., Monaghan, A.P., John, B., and Milos, P.M. (2010). Comprehensive polyadenylation site maps in yeast and human reveal pervasive alternative polyadenylation. *Cell* 143, 1018–1029.

Robinson, M.D., McCarthy, D.J., and Smyth, G.K. (2010). edgeR: a Bioconductor package for differential expression analysis of digital gene expression data. *Bioinformatics* 26, 139–140.

- Schultz, J.M., Yang, Y., Caride, A.J., Filoteo, A.G., Penheiter, A.R., Lagziel, A., Morell, R.J., Mohiddin, S.A., Fananapazir, L., Madeo, A.C., et al. (2005). Modification of human hearing loss by plasma-membrane calcium pump PMCA2. *N. Engl. J. Med.* 352, 1557–1564.
- Shepard, P.J., Choi, E.-A., Lu, J., Flanagan, L.A., Hertel, K.J., and Shi, Y. (2011). Complex and dynamic landscape of RNA polyadenylation revealed by PAS-Seq. *RNA* 17, 761–772.
- Shi, Y. (2012). Alternative polyadenylation: new insights from global analyses. *RNA* 18, 2105–2117.
- Shi, Y., Di Giammartino, D.C., Taylor, D., Sarkeshik, A., Rice, W.J., Yates, J.R., 3rd, Frank, J., and Manley, J.L. (2009). Molecular architecture of the human pre-mRNA 3' processing complex. *Mol. Cell* 33, 365–376.
- Smibert, P., Miura, P., Westholm, J.O., Shenker, S., May, G., Duff, M.O., Zhang, D., Eads, B.D., Carlson, J., Brown, J.B., et al. (2012). Global patterns of tissue-specific alternative polyadenylation in *Drosophila*. *Cell Rep.* 1, 277–289.
- Smrt, R.D., Szulwach, K.E., Pfeiffer, R.L., Li, X., Guo, W., Pathania, M., Teng, Z.-Q., Luo, Y., Peng, J., Bordey, A., et al. (2010). MicroRNA miR-137 regulates neuronal maturation by targeting ubiquitin ligase mind bomb-1. *Stem Cells* 28, 1060–1070.
- Strehler, E.E., and Zacharias, D.A. (2001). Role of alternative splicing in generating isoform diversity among plasma membrane calcium pumps. *Physiol. Rev.* 81, 21–50.
- Takagaki, Y., and Manley, J.L. (1997). RNA recognition by the human polyadenylation factor CstF. *Mol. Cell. Biol.* 17, 3907–3914.
- Tan, C.L., Plotkin, J.L., Venø, M.T., von Schimmelmann, M., Feinberg, P., Mann, S., Handler, A., Kjems, J., Surmeier, D.J., O'Carroll, D., et al. (2013). MicroRNA-128 governs neuronal excitability and motor behavior in mice. *Science* 342, 1254–1258.
- Tian, B., and Manley, J.L. (2013). Alternative cleavage and polyadenylation: the long and short of it. *Trends Biochem. Sci.* 38, 312–320.
- Ulitisky, I., Shkumatava, A., Jan, C.H., Subtelny, A.O., Koppstein, D., Bell, G.W., Sive, H., and Bartel, D.P. (2012). Extensive alternative polyadenylation during zebrafish development. *Genome Res.* 22, 2054–2066.
- Utomo, A.R., Nikitin, A.Y., and Lee, W.H. (1999). Temporal, spatial, and cell type-specific control of Cre-mediated DNA recombination in transgenic mice. *Nat. Biotechnol.* 17, 1091–1096.
- Venkataraman, K., Brown, K.M., and Gilmartin, G.M. (2005). Analysis of a non-canonical poly(A) site reveals a tripartite mechanism for vertebrate poly(A) site recognition. *Genes Dev.* 19, 1315–1327.
- Wang, L., Dowell, R.D., and Yi, R. (2013). Genome-wide maps of polyadenylation reveal dynamic mRNA 3'-end formation in mammalian cell lineages. *RNA* 19, 413–425.
- Weyn-Vanhentenryck, S.M., Mele, A., Yan, Q., Sun, S., Farny, N., Zhang, Z., Xue, C., Herre, M., Silver, P.A., Zhang, M.Q., et al. (2014). HITS-CLIP and integrative modeling define the Rbfox splicing-regulatory network linked to brain development and autism. *Cell Rep.* 6, 1139–1152.
- Yao, C., Biesinger, J., Wan, J., Weng, L., Xing, Y., Xie, X., and Shi, Y. (2012). Transcriptome-wide analyses of CstF64-RNA interactions in global regulation of mRNA alternative polyadenylation. *Proc. Natl. Acad. Sci. USA* 109, 18773–18778.
- Yao, C., Choi, E.-A., Weng, L., Xie, X., Wan, J., Xing, Y., Moresco, J.J., Tu, P.G., Yates, J.R., 3rd, and Shi, Y. (2013). Overlapping and distinct functions of CstF64 and CstF64 τ in mammalian mRNA 3' processing. *RNA* 19, 1781–1790.
- Zhang, Y., Chen, K., Sloan, S.A., Bennett, M.L., Scholze, A.R., O'Keefe, S., Phatnani, H.P., Guarnieri, P., Caneda, C., Ruderisch, N., et al. (2014). An RNA-sequencing transcriptome and splicing database of glia, neurons, and vascular cells of the cerebral cortex. *J. Neurosci.* 34, 11929–11947.